UV photodissociation spectroscopy of cryogenic cooled gas phase host-guest complex ions of crown ethers

Yoshiya Inokuchi, Takeharu Haino, Ryo Sekiya, Fumiya Morishima, Claude Dedonder, Géraldine Féraud, Christophe Jouvet, Takayuki Ebata

UV photodissociation spectroscopy of cryogenic cooled gas phase host-guest complex ions of crown ethers

Yoshiya Inokuchi[1], Takeharu Haino[1], Ryo Sekiya[1], Fumiya Morishima[1], Claude Dedonder[2], Géraldine Féraud[2], Christophe Jouvet*[2], and Takayuki Ebata*[1]

[1]Department of Chemistry, Graduate School of Science, Hiroshima University, Higashi-Hiroshima 739-8526, Japan

[2]CNRS, Aix Marseille Université, Physique des Interactions Ioniques et Moléculaires (PIIM) UMR 7345, 13397 Marseille cedex, France

Abstract:

The geometric and electronic structures of cold host-guest complex ions of crown ethers (CEs) in the gas phase have been investigated by ultraviolet (UV) fragmentation spectroscopy. As host CEs, we chose 15-crown-5 (15C5), 18-crown-6 (18C6), 24-crown-8 (24C8), and dibenzo-24-crown-8 (DB24C8), and as guests protonated-aniline (aniline•H^+) and protonated-dibenzylamine (dBAM•H^+) were chosen. The ions generated by an electrospray ionization (ESI) source were cooled in a quadrupole ion-trap (QIT) by cryogenic cooler, and the UV spectra were obtained by UV photodissociation (UVPD) spectroscopy. The UV spectroscopy was complemented by quantum chemical calculations of the most probable complex structures. The UV spectrum of aniline•H^+•CE is very sensitive to the symmetry of CE; aniline•H^+•18C6 shows sharp electronic spectrum similar to aniline•H^+, while aniline•H^+•15C5 shows very broad structure with poor Franck-Condon factors. In addition, a remarkable cage effect in the fragmentation process after UV excitation was observed in both complex ions. In the aniline•H^+•CE complexes, the cage effect completely removed the dissociation channels of the aniline•H^+ moiety. A large difference in the fragmentation yield between dBAM•H^+•18C6 and dBAM•H^+•24C8 was observed due to a large barrier for releasing dBAM•H^+ from the axis of rotaxane in the latter complex.

Introduction:

Crown ethers (CEs) are macrocyclic ethers built with oxyethylene (-CH_2-CH_2-O-) units. Pedersen synthesized the first crown ether (CE), dibenzo-18-crown-6 (DB18C6) in 1967, and investigated complexation with various metal salts[1,2] using UV spectroscopy. Since then, CEs have been playing an important role in host-guest and supramolecular chemistry. CEs can include not only metal ions in their cavity but form various complexes with ionic and neutral species through non-covalent interactions. Applications of CEs as molecular receptors, metal cation extraction agents, fluoroionophores and phase transfer catalytic media have been described in a number of studies.[3-14] Especially, it is well known that, in condensed phase, CEs exhibit selectivity when they include the guest species.[9-14] This selectivity is described by the matching between the size of the guest species and that of the CE cavity. On the other hand, the host-guest binding energy measured in the gas phase shows different characteristics from those observed in the condensed phase.[15-17] This discrepancy requires to search more information on the intrinsic nature of CEs, such as flexibility of the CE frame and conformation preference, as well as solvent effects on the stability of the inclusion complexes.

To investigate the difference between condensed phase and gas phase studies and to obtain information on the host-guest interaction at the microscopic level, we have been studying the structures, conformation preference, and selectivity of guests for the inclusion complexes of CEs in the gas phase.[18-27] The cold gas phase complexes are generated either in using supersonic expansion technique for neutral complexes[18-24] or with eletrospray ionization (ESI)/Cold ion-trap method for ionic complexes.[24-27] We apply various laser spectroscopic methods to measure conformer specific UV and IR

spectra, and the spectra are analyzed by comparing the spectra with those of possible complexes obtained by quantum chemical calculations. Based on these studies, we reported that the conformations of CEs in the inclusion complexes are generally different from the most stable conformer of bare forms, because CEs will change their structures so that they can include the different size and structure of guest species in their cavities.[20,22,23]

In the present work, we report a study on host-guest complexes of CEs with protonated aromatic amines. CEs can be good receptors of protonated amines since stable complexes can be formed via multiple NH•••O hydrogen bonds. First, we investigate the inclusion complexes of protonated aniline (aniline•H^+) with 18-crown-6 (18C6) and 15-crown-5 (15C5). These complexes have the structure in which the NH_3^+ group of aniline•H^+ (guest) is bonded to 18C6 or 15C5 (host) through N–H•••O hydrogen bonds. In the previous study, we reported that UV photodissociation (UVPD) of aniline•H^+ generates aniline$^+$ and $C_6H_5^+$ fragment ions.[28] Here we examine how the complex formation affects the electronic spectrum of aniline•H^+ as well as the UVPD pattern. Second, we report the host-guest complexes between protonated dibenzylamine (dBAM•H^+) with 18C6, 24-crown-8 (24C8), and dibenzo-24-crown-8 (DB24C8). dBAM•H^+ is used as an axis molecules of rotaxane. Rotaxane molecules have attracted great interest for their potential use in molecular machines, such as molecular switches[29-33] and molecular shuttles.[34-36] In this study, we recorded the UV electronic spectra and the fragmentation yield after UV excitation for the complexes between dBAM•H^+ and 18C6, 24C8 and DB24C8. We investigate how the complex or rotaxane formation changes the electronic structure of the constituent chromophores and UVPD

pattern by comparing the observed spectra with those of the possible structures obtained by quantum chemical calculations.

Experimental and computational:

Experimental setup

The experimental setup has been described in previous papers.[28,37,38] The setup consists of three parts: an ESI source, a cryogenically cooled quadrupole-ion-trap (QIT) and a time-of-flight mass spectrometer (TOF-Mass).[39,40] Protonated ions are produced in the ESI source[41] and trapped in an octopole trap at the exit of the capillary. They are extracted by a negative electric pulse and are further accelerated by a second electric pulse just after the exit electrode. The ions are driven by a couple of electrostatic lenses toward the Paul trap. A mass gate at the entrance of the trap selects the parent ion. The ions are trapped in the Paul trap cooled by a cryostat (Coolpak Oerlikon) and filled with helium buffer gas injected with a pulsed valve. The ions are thermalized at around 30 K while they stay in the trap. After 60 ms, the pump UV laser is introduced to dissociate the cold ions, and after another 30 ms the fragments and remaining parent ions are extracted to the TOF spectrometer and are detected on a microchannel plates (MCP) detector. The UV spectrum is obtained by scanning the laser frequency and recording the ion fragments on the MCP detector. We use an OPO laser (EKSPLA model-NT342B) as the UV light source, and its spectral resolution is 8 cm^{-1}. The unfocused laser is shaped to a 2 mm^2 spot in the trap, corresponding to a power of c.a. 5 mW.

Computational

For the structural calculation of dBAM•H^+, and complexes of aniline•H^+ and dBAM•H^+ with crown ethers, possible conformers were first searched by selecting some initial geometries optimized at the AM1 level[42], and the obtained structures were optimized with density functional theory calculations using M05-2X/6-31+G*.

To obtain plausible structures for DB24C8•H^+ and dBAM•H^+•DB24C8 complex, we first used a classical force field to search initial conformations. We performed a Monte Carlo simulation by mixed torsional search with low-mode sampling in MacroModel[43] V.9.1 with MMFF94s force field[44], and optimized the geometries by Polak-Ribiere conjugate gradient algorithm (PRCG) algorithm[45] with a convergence threshold of 0.05 kJ/mol. From this calculation, 10 isomers for the DB24C8•H^+ complex and 3 isomers for dBAM•H^+•DB24C8 were obtained within 10 kJ/mol of the most stable one. All these isomers were geometry-optimized by DFT calculations at the M05-2X/6-31+G* level with *loose* optimization criteria. Quantum chemical calculations were performed in the Gaussian 09 program package. [46]

Synthesis of materials

Dibenzylammonium hexafluorophosphate (dBAM•H^+•PF_6^-): dBAM•H^+•PF_6^- was synthesized by a previously reported procedure by Ashton et al.[47] Aqueous hydrogen chloride (1 mol L^{-1}, 26.1 mL) was added to dibenzylamine (26.1 mmol), and the solution was stirred for 1.5 h at room temperature. The solvent was removed under vacuum and the residue was dissolved in hot deionized water (100 mL, 70 °C). Saturated aqueous ammonium hexafluorophosphate was added until no further

precipitation occurred. The white solid was filtered off and dried to afford the desired product 8.34 g (93 %).

Pseudo-rotaxanes: dBAM•H^+•DB24•PF_6^- was prepared from DB24C8 and dBAM•H^+•PF_6^-. DB24C8 (100 mg, 0.222 mmol) was dissolved in chloroform (10 mL), and then dBAM•H^+•PF_6^- salt (76.6 mg, 0.223 mmol) was added. After being stirred for 1h at room temperature, the mixture was concentrated in *vacuo* to afford the pseudo-rotaxane 167 mg (94 %) as a white solid.

dBAM•H^+•24C8•PF_6^- was prepared from 24C8 and dBAM•H^+•PF_6^-. 24C8 (72.0 mg, 0.204 mmol) was dissolved in chloroform (5 mL), and then dBAM•H^+•PF_6^- salt (70.1 mg, 0.204 mmol) was added. After being stirred for 0.5 h at room temperature, the mixture was concentrated in *vacuo* to afford the pseudo-rotaxane 132 mg (93 %) as a white solid.

The rotaxane formation was confirmed using dBAM•H^+ NMR spectroscopy. The catechol protons split two resonances, one of which was slightly upfield-shifted. Two sets of the oxymethylene protons of DB24C8 showed the up-field shifts of 0.16 and 0.05 ppm, respectively. Two benzene rings of bound dBAM•H^+•PF_6^- face one another as found in the crystal structure. The crown moiety is placed within the cleft of the benzene rings; therefore, the aromatic shielding most likely resulted in the up-field shifts of the crown protons. The similar chemical shift change was observed in the ^{1}H NMR spectrum of dBAM•H^+•24C8•PF_6^-. The oxyethylene protons of 24C8 showed the up-field shift of 0.19 ppm. These evidences are consistent with those reported by Ashton et al. [47]

Results and discussion

1. Protonated aniline • crown ether complex ion

Left panel of Fig. 1 shows the UVPD spectra of (a) aniline•H^+, (b) aniline•H^+•18C6, and (c) aniline•H^+•15C5 ions in the 35000–44000 cm^{-1} region. The excess proton in aniline•H^+ is attached to the amino group, forming the anilinium ion, $C_6H_5NH_3^+$. The right panel of Fig. 1 shows the time of flight (TOF) spectra of aniline•H^+ without (blue) and with UV (red) laser irradiation. As seen in the figure, the main photofragment ions for aniline•H^+ are aniline$^+$ (m/z = 93) and $C_6H_5^+$ (m/z = 77), produced by H atom loss of or NH_3 loss, respectively.[45] The UVPD spectrum of the aniline•H^+ ion shows a band origin at 38215 cm^{-1}, which is ~4200 cm^{-1} blue-shifted as compared to the transition origin of neutral aniline (34027 cm^{-1}).[48] This blue shift between the transitions of ionic and neutral species is the largest observed for the systems investigated here. It can be assigned to the deconjugation of the nitrogen lone pair when H^+ attaches to the amino group so that aniline•H^+ has a toluene like electronic structure (the (0,0) band of the toluene S_1-S_0 transition is located at 37477 cm^{-1}).[4649] A progression on a mode of ~920 cm^{-1} can be followed starting from the band origin, as shown with solid lines in Fig. 1a, which is assigned to the ring breathing mode (mode 1).[50] This frequency is closer to that of neutral toluene (935 cm^{-1}) than that of aniline (952 cm^{-1}).

In the case of the aniline•H^+•18C6 complex, two sharp bands are observed at 38565 and 38640 cm^{-1} (Fig. 1b). Since one cannot see any strong band or progression around these two bands, they may probably be ascribed to the origin band of two different isomers. The position of the origin bands is much closer to that of aniline•H^+ than to that of neutral aniline, thus the proton is still located on the amino group of the aniline

part. The UVPD spectrum of aniline•H^+•18C6 also shows a progression with an interval of ~920 cm^{-1} similar to aniline•H^+ as highlighted by solid lines in Fig. 1b, although the transitions to higher vibrational levels show broadened features. Since the frequency of the ring breathing mode is almost the same for aniline•H^+ and aniline•H^+•18C6 ions, the benzene ring in the aniline•H^+•18C6 ion seems not to be strongly affected by the 18C6 part. The right panel of Fig. 1 shows the TOF spectra of aniline•H^+•18C6. We find the fragment pattern is quite different from that of aniline•H^+. Three photofragment ions are observed for aniline•H^+•18C6; 18C6•H^+ (m/z = 265), $(OCH_2CH_2)_4$•H^+ (m/z = 177), and $(OCH_2CH_2)_3$•H^+ (m/z = 133); no fragment ion due to the dissociation of the aniline•H^+ part, H loss (dissociation of an NH bond) or NH_3 loss (dissociation of the CN bond), is seen. The CN bond breaking observed in the UVPD of aniline•H^+ could lead to formation of the CE•NH_3^+ fragment, but is not observed either. The fragmentation pattern rather indicates that a proton transfer occurs from aniline•H^+ to 18C6 after the UV excitation, and the excess energy initially injected in the aniline•H^+ part efficiently flows to the 18C6 part. After UV excitation, the aniline•H^+•18C6 complex may relax to the ground state and transfer a proton and energy to the 18C6 part, leading to fragmentation in aniline and 18C6•H^+. 18C6•H^+ has enough internal energy to further fragment into $(OCH_2CH_2)_4$•H^+ or $(OCH_2CH_2)_3$•H^+ as observed. Thus, 18C6 has a role of reservoir of energy; the energy initially imparted by the optical excitation into electronic and vibrational energy of the aniline part is transferred to 18C6, a kind of cage effect. As shown in Fig. 1S in the Supporting Information, the intensity of the $(OCH_2CH_2)_4$•H^+ fragment ion becomes stronger than that of 18C6•H^+ with increasing the UV photon energy; the formation of $(OCH_2CH_2)_4$•H^+ requires more energy than that of 18C6•$H^+$and the fragmentation occurs statistically after the proton and energy transfer from

aniline•H^+ to 18C6.

In contrast to aniline•H^+ and aniline•H^+•18C6, the UVPD spectrum of aniline•H^+•15C5 (Fig. 1c) shows a broad absorption in the region of 39000–44000 cm^{-1}. In aniline•H^+•15C5, the proton is attached to the NH_2 group of the aniline part as in aniline•H^+•18C6. However, the UV spectrum of the aniline•H^+•15C5 ion is quite different from that of aniline•H^+•18C6, which may imply poor Franck-Condon overlap between the S_0 and S_1 states.

Fig. 2 shows the typical structures of (a) aniline•H^+•18C6 and (b) aniline•H^+•15C5 complexes. In the aniline•H^+•18C6 complex, the NH_3^+ group is bonded to 18C6 through three N–H•••O hydrogen bonds as was expected. This intermolecular bond seems to result in effective proton transfer from aniline•H^+ to 18C6 after the UV excitation. The H•••O distances are almost the same (~1.83 Å) for all the three hydrogen bonds; the 18C6 cavity seems well fitted to the NH_3^+ group. The 18C6 component and the aromatic ring are located apart, so that there is no strong intermolecular interaction between 18C6 and the benzene ring, which is consistent with the similar frequency observed in the UVPD spectra of aniline•H^+ and aniline•H^+•18C6 ions for the benzene breathing-mode. The proton transfer from aniline•H^+ to 18C6 after UV excitation of the complex is understood in terms of larger proton affinity (PA) of the crown ether (967.0 kJ/mol) than that of aniline (882.5 kJ/mol).[51] After UV excitation, the proton transfer occurs from aniline•H^+ to 18C6 in the S_1 excited state of the complex or after the relaxation to S_0 by internal conversion (IC).

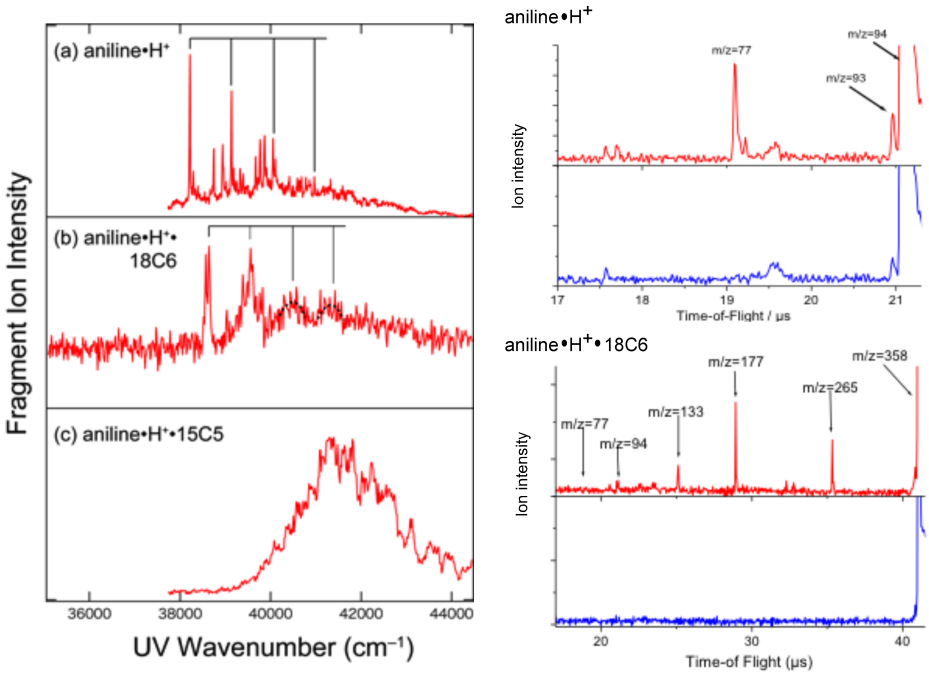

Fig. 1. (left) UVPD spectra: (a) aniline•H^+, (b) aniline•H^+•18C6, and (c) aniline•H^+•15C5. (right) TOF spectra of aniline•H^+ and aniline•H^+•18C6, without UV irradiation (blue) and with UV irradiation fixed at the band origins (red). The solid black lines in figure 1a and 1b show the progression with an interval of ~920 cm^{-1} assigned to the ring breathing mode.

For the aniline•H^+•15C5 complex, the proton is also initially situated on the aniline molecule, and the aniline•H^+ ion is bonded to 15C5 through two N–H•••O hydrogen bonds, instead of three H-bonds in aniline•H^+•18C6. The PA of 15C5 is 943.8 kJ/mol,[48] larger than that of aniline; thus, after UV excitation, the proton of aniline•H^+ is also transferred to 15C5. The difference in the UV spectral patterns between the aniline•H^+•18C6 and aniline•H^+•15C5 ions can be assigned to the asymmetry of the hydrogen bond network in the aniline•H^+•15C5 ion that distorts the structure of the complex and leads to a change in geometry between the ground and excited states, which results in poor Franck-Condon overlap in the UVPD spectrum (Fig. 2b). Another possibility to explain the broad feature of the UV spectrum of aniline•H^+•15C5 is the

coexistence of other isomer(s) in aniline•H^+•15C5. Pasker *et al*. investigated aniline•H^+ and its complexes by infrared photo-dissociation (IRPD) spectroscopy and theoretical calculations,[52] and reported that aniline•H^+ has two almost equally stable isomers, the ammonium and carbenium isomers, and that their relative population changes with complexation. It may be possible that the asymmetrical hydrogen-bonding of the aniline•H^+•15C5 complex induces a larger population of the carbenium isomers, which should have different vibronic structures than the ammonium type isomer. However, calculations show that the ground state carbenium complex with 15C5 is more than 1 eV higher in energy than the anilinium•15C5 complex, because in the carbenium ion the positive charge is largely delocalized whereas in the ammonium ion the charge is well localized on the ammonium group.

The UV excitation does not produce any fragment ion via the loss of H atom or NH_3 loss neither in aniline•H^+•18C6 nor in aniline•H^+•15C5, which differs from the UVPD of bare aniline•H^+. The crown ether induced cage effect on the fragmentation of anilinium is surprising. While it is easy to understand that the cage will suppress the H loss channel from anilinium, the absence of the NH_3 loss channel, which is one of the major fragments in the anilinium ion, is unexpected. This is in contrast to the protonated tryptamine case in which the C-NH_3 bond breaking is observed in both the free ion[53] and in the complex with 18C6. [54] In the complex, this fragmentation channel was assigned to an excited state dissociation, which thus seems absent in anilinium•CE complexes.

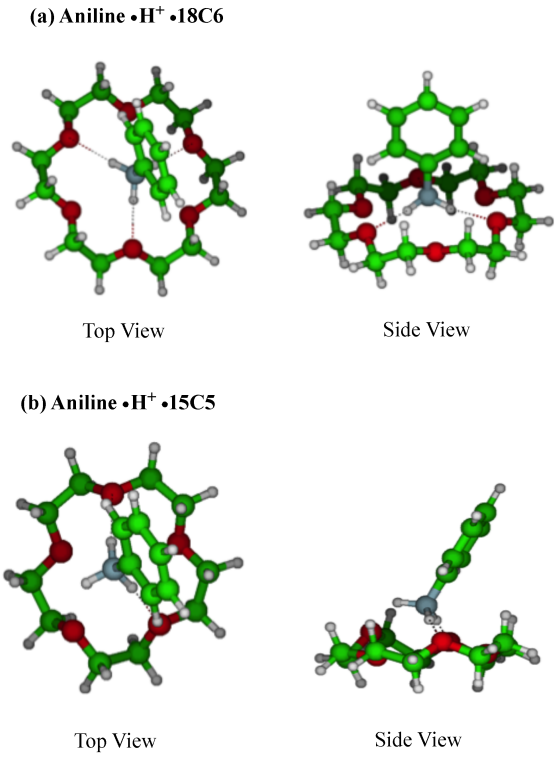

Fig. 2. Typical stable geometries of (a) aniline•H^+•18C6 and (b) aniline•H^+•15C5.

2. Protonated dibenzylamine (dBAM•H^+)

Protonated dibenzylamine (dBAM•H^+) is used as an axis molecule in pseudo rotaxane. We investigate how the rotaxane formation affects the electronic transition of dBAM•H^+. Fig. 3 shows the UVPD spectrum of dBAM•H^+ obtained by monitoring the m/z =107 ($C_7NH_9^+$) major fragment. The spectrum is essentially the same as that reported in our previous paper,[38] except the spectrum is recorded in a wider energy region. A sharp (0,0) band appears at 37450 cm^{-1} (band A) along with several sharp vibronic bands involving torsional mode (170 cm^{-1}) and skeletal modes (550, 745, 930 and 1540 cm^{-1}). The vibronic structure corresponding to skeletal modes is very similar to that of aniline•H^+. Additionally, a weak band (band B) is observed at 70 cm^{-1} on the lower frequency side of band A. We investigated the temperature dependence of bands A and B, and found that the relative intensity of band B with respect to band A

increases with the increase of the temperature of the trap (See Supporting Material Fig. 2S). Thus band B is due either to a hot band or to a higher energy conformer (open conformer).

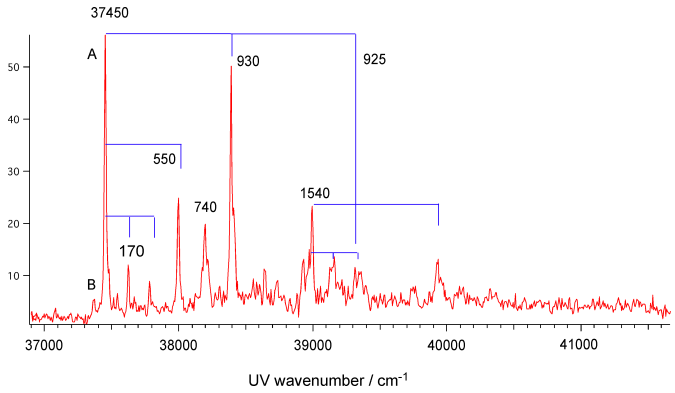

Fig. 3. UVPD spectrum of cold protonated dibenzylamine (dBAM•H^+) in the gas phase.

Possible structures of dBAM•H^+ have been investigated by DFT calculations at the M05-2X/6-31G* level. Three stable conformers were obtained: (1) open conformer, (2) twisted conformer, and (3) stacked conformer as shown in Fig. 4. Table 1 shows their relative ground state and vertical excitation energies. Conformers (1) and (2) have very similar ground state energies; conformer (2) being 4.3 kJ/mol higher than conformer (1) without zero point energy (ZPE) correction. Conformer (3) has a higher energy (85.4 kJ/mol), and is not expected to be present in the trap. Since dBAM•H^+ has two benzene chromophores, we expect two closely lying electronic states, S_1 and S_2, corresponding to the excitation of each of the two chromophores. In the UVPD spectrum, a strong band A and weak band B are observed. Since they show different temperature dependence, band A can be assigned to the most stable open conformer and band B to the twisted conformer. Table 1 also lists the vertical excitation energies to S_1 and S_2 states and their oscillator strengths calculated by TD-DFT calculation at the

M05-2X/6-31G* level. As seen in Table 1, S_1 and S_2 states are located at almost the same energy for the open and twisted conformers, and the oscillator strength of the S_1-S_0 transition of the open conformer is zero, which is due to the cancelation of the transition dipoles of the constituent two benzene chromophores. The calculated results are in accordance with the observation of a single band origin, band A, in the UVPD spectrum corresponding to the open conformer, and a weak band B corresponding to the twisted conformer.

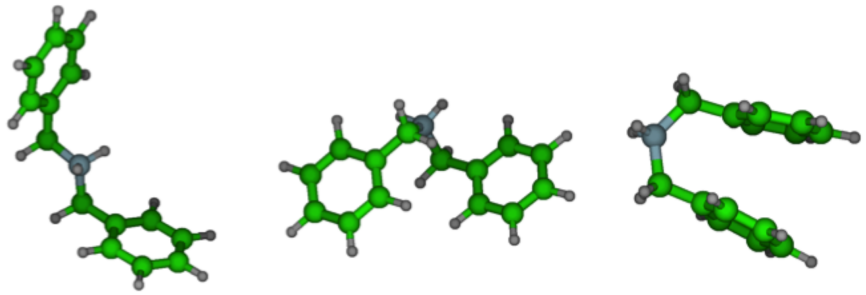

Fig. 4 Optimized structures of dBAM•H^+ conformers at the M05-2X/6-31G* level.

Table 1. Relative ground state stabilization energies (kJ/mol), vertical excitation energies (eV) and oscillator strength (parentheses) for the three dBAM•H^+ conformers calculated at the M05-2X/6-31G*level.

Conformer	open	twisted	stacked
S_0(kJ/mol)	0	4.3	85.4
S_1(eV)	5.57(0.0)	5.56(2.0E-4)	4.93(0.0)
S_2(eV)	5.58(9.8E-3)	5.57(8.1E-3)	5.12(3.9E-2)

3. Complexes of dBAM•H$^+$ with 18C6 and 24C8

dBAM•H$^+$ does not go through the 18C6 ring due to steric hindrance, but dBAM•H$^+$ can go through the 24C8 ring to form a pseudo-rotaxane.[47] So, we investigated how the difference of complex structure will be reflected in the UV spectra and fragmentation yields of the two complexes.

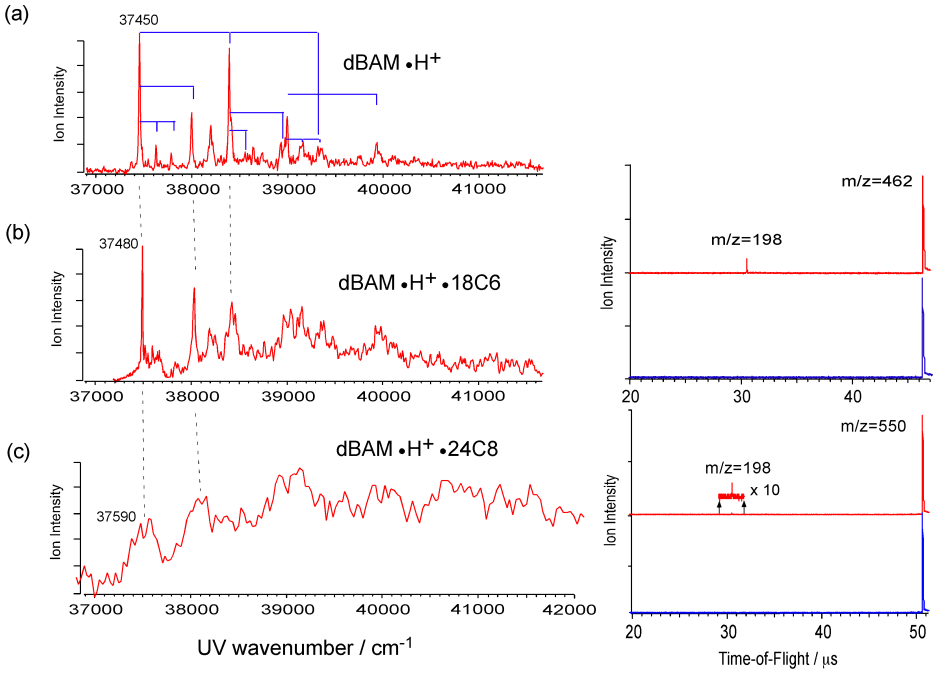

Fig. 5. (a) UVPD spectrum of dBAM•H$^+$. (b) (left) UVPD spectrum of dBAM•H$^+$•18C6. (right) TOF spectrum without UV irradiation (blue) and with UV fixed at 37481 cm^{-1} (red). The ion intensity is normalized relative to that of parent ion intensity. (c) (left) UVPD spectrum of dBAM•H$^+$•24C8. (right) TOF spectrum without UV irradiation (blue) and with UV fixed at 37594 cm^{-1} (red). The ion intensity is normalized relative to that of parent ion intensity.

Figs. 5b and 5c show the UVPD spectra of dBAM•H$^+$•18C6 and dBAM•H$^+$•24C8 complex ions. At the opposite of the aniline•H$^+$•18C6 UVPD, we observed dBAM•H$^+$ fragment ions (m/z = 198) instead of CE•H$^+$ in both cases (see the TOF spectra on the right panels of Fig. 5), and the UVPD spectra are recorded by monitoring the dBAM•H$^+$ fragment in both cases. The PA value of dBAM is not known, but that of benzylamine

is reported to be 913 kJ/mol. Since we do not observe the 18C6•H^+ fragment, the PA of dBAM should be larger than that of 18C6 (967 kJ/mol). The UVPD spectra of dBAM•H^+•18C6 and dBAM•H^+•24C8 are compared to the UVPD spectrum of dBAM•H^+ (Fig. 5a). The (0,0) band of dBAM•H^+•18C6 is located at 37481 cm^{-1}, 28 cm^{-1} blue-shifted from dBAM•H^+ and the overall structure of the spectrum is very similar to that of dBAM•H^+ except that higher vibronic bands are broadened. This situation is the same as between aniline•H^+ and aniline•H^+•18C6. The UVPD spectrum of dBAM•H^+•24C8 is much weaker and broader and its band origin is located at around 37590 cm^{-1}. Thus, the difference in the complex structure between dBAM•H^+•18C6 and dBAM•H^+•24C8 is not reflected in the electronic transition origins, which are almost the same, but in the width of the vibronic structures. However, the main difference is observed in the UV photo-fragmentation yield. The right panels of Figs. 5b and 5c show the TOF spectra of dBAM•H^+•18C6 and dBAM•H^+•24C8 with and without the photodissociation laser, the UV frequency being fixed on the band origin of each complex. By comparing the two TOF spectra, the relative fragmentation yield giving dBAM•H^+ from dBAM•H^+•18C6 is much larger than that from dBAM•H^+•24C8 under the same UV laser power conditions. Since the UV absorption cross sections are similar between dBAM•H^+•18C6 (calculated oscillator strength of 1.4×10^{-3}) and dBAM•H^+•24C8 complexes (oscillator strength 2×10^{-3}), the small fragmentation yield in the latter case is assigned to a barrier for releasing dBAM•H^+ from the 24C8 cavity in the dBAM•H^+•24C8 pseudo rotaxane.

It is very difficult to determine the structures of dBAM•H^+•18C6 and dBAM•H^+•24C8 from the electronic spectra. However, the number of possible isomers should be reduced because of the low temperature of the trap (30 K). Actually, as seen

in Fig. 5b, the UVPD spectrum of dBAM•H^+•18C6 shows a single sharp band origin. Thus, by assuming that the oscillator strengths of the conformers are not different so much from each other, only one major conformer is observed under the present conditions. Fig. 6 shows typical ground state optimized structures for (a) dBAM•H^+•18C6 and (b) dBAM•H^+•24C8. For dBAM•H^+•18C6, a twisted shaped dBAM•H^+ is attached above 18C6 and bound to two ether oxygen atoms via NH•••O H-bonds. In the dBAM•H^+•24C8 complex, on the other hand, dBAM•H^+ goes through the 24C8 cavity forming pseudo-rotaxane. The calculated binding energy is 236 kJ/mol for dBAM•H^+•18C6, and 264 kJ/mol for dBAM•H^+•24C8 at the M05-2X/6-31G* level with BSSE correction. Thus, though the binding energy is not so different between dBAM•H^+•18C6 and dBAM•H^+•24C8, the low fragmentation yield of dBAM•H^+•24C8 may come from a larger barrier for dBAM•H^+ to be released from the 24C8 cavity.

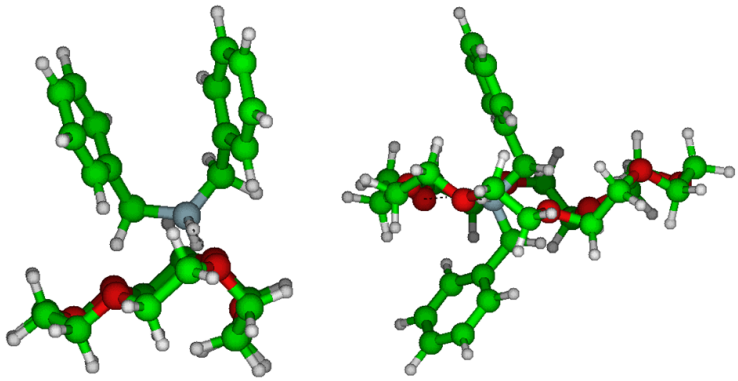

Fig. 6. Optimized structures of (a) dBAM•H^+•18C6 and (b) dBAM•H^+•24C8 complexes at the M05-2X/6-31G* level of calculation.

4. dBAM•H^+•DB24C8 pseudo–rotaxane

Fig. 7b shows the UVPD spectrum of dBAM•H^+•DB24C8 pseudo–rotaxane measured at 30 K. The spectrum is compared with that of dBAM•H^+ (Fig. 7a), and

DB24C8•H^+ (Fig. 7c), respectively. The spectrum of dBAM•H^+•DB24C8 shows broad structures with a band origin at ~36350 cm^{-1}. It is not clear whether the broadness is due to the overlap of the transitions of several coexisting isomers or to spectral congestion due to low vibrational modes. The first band is more than 1000 cm^{-1} red-shifted as compared to the (0,0) transition of dBAM•H^+, and is rather close to the (0,0) band of DB24C8•H^+ (36050 cm^{-1}). This suggests that the electronic transition of dBAM•H^+•DB24C8 in this region is not due to dBAM•H^+ but to DB24C8 or DB24C8•H^+. For comparison, Fig. 7d shows the laser induced fluorescence spectrum of the S_1-S_0 transition of jet-cooled neutral DB24C8 in the band origin region. For neutral DB24C8, two different conformers were identified at 35195 and 35408 cm^{-1}, which were assigned to the chair and boat forms, respectively.[21] The S_1-S_0 electronic transition of DB24C8•H^+ is roughly 800 cm^{-1} blue-shifted with respect to that of neutral DB24C8. Thus, the spectrum of dBAM•H^+•DB24C8 in this region is assigned to excitation of the DB24C8•H^+ chromophore. The intensity of the dBAM•H^+ fragment at m/z = 198 from the dBAM•H^+•DB24C8 photodissociation is 10–20 times larger than from the dBAM•H^+•24C8 photodissociation although these complexes have similar pseudo-rotaxane structures. The difference is due to the larger absorption cross-section of the DB24C8•H^+ chromophore as compared to the dBAMH^+ absorption, as will be discussed later (Table 2).

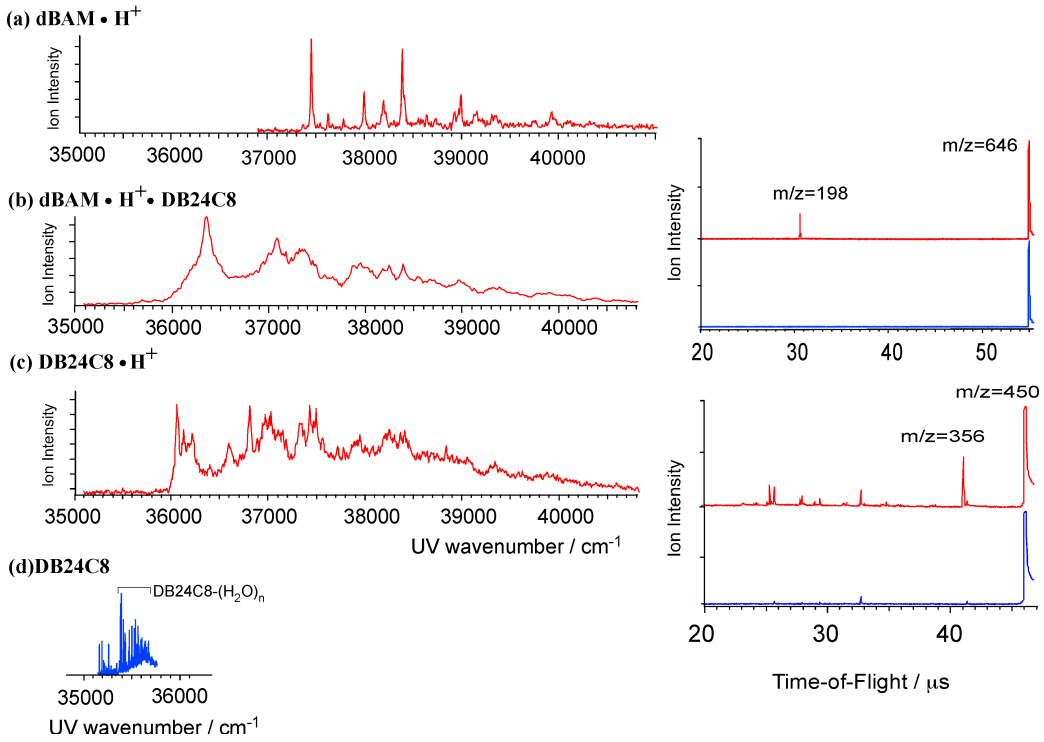

Fig. 7. (a) UVPD spectrum of dBAM•H^+. (b) (left) UVPD spectrum of dBAM•H^+•DB24C8. (right) TOF spectrum of dBAM•H^+•DB24C8 without UV irradiation (blue) and with UV fixed at 36350 cm^{-1} (red). The ion intensity is normalized relative to that of parent ion intensity. (c) (left) UVPD spectrum of DB24C8•H^+ observed by monitoring m/z = 356 fragment ion. (right) TOF spectrum of DB24C8•H^+ without UV irradiation (blue) and with UV fixed at 36050 cm^{-1} (red). The intensity of DB24C8•H^+ is largely out of scale to expand the weak fragment ion signals. (d) LIF spectrum of DB24C8 in a supersonic jet.

We calculated possible initial structures of DB24C8•H^+ and dBAM•H^+•DB24C8 by MMF calculations further optimized with DFT calculations at the M05-2X/6-31+G* level. Fig. 8 shows the two most stable structures of DB24C8•H^+. Other conformers are more than 2.6 kJ/mol higher in energy and their structures are shown in Fig. S3. In isomer 1, a proton is bound in a bifurcated manner to two ether oxygen atoms, one of which is adjacent to a benzene ring. Isomer 2 has a covalent O-H^+ bond and the proton is H-bonded to an opposite ether oxygen. The DB24C8•H^+ S_1-S_0 electronic transition is more than 800 cm^{-1} blue-shifted as compared to the neutral DB24C8 transition, which is

compatible with the structure of isomer 1, because its electronic transition should be most affected by the proton binding to the oxygen atom adjacent to one benzene ring in this structure. Fig. 9 shows the most stable structure calculated for the dBAM•H^+•DB24C8 complex. The next stable isomer is more than 5 kJ/mol higher in energy (See Fig. S4 in Supporting Information). In the most stable structure, DB24C8 has a boat-structure and the benzene rings form quasi π–π stacking structure with one of the dBAM benzene rings. In addition, one NH bond of dBAM is H-bonded to an oxygen atom adjacent to a DB24C8 benzene ring. This situation is essentially the same as in the most stable structure (Isomer 1) of DB24C8•H^+.

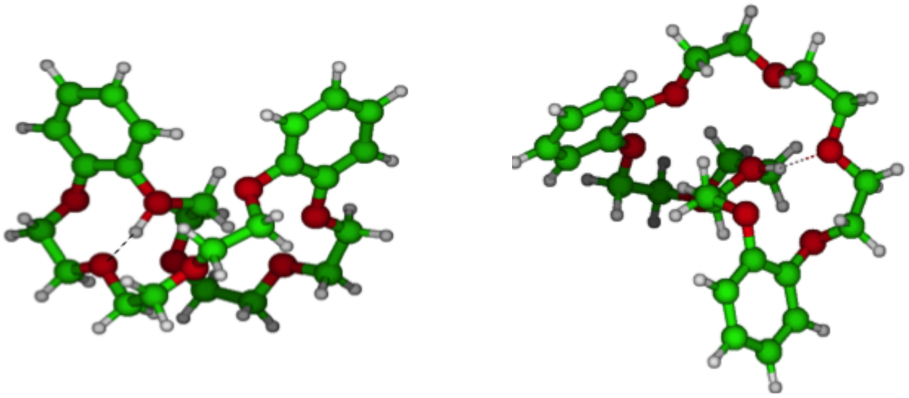

Isomer 1 (0 kJ/mol) **Isomer 2 (1.39 kJ/mol)**

Fig. 8. Two lowest energy isomers of DB24C8•H^+ obtained at the M05-2X/6-31+G* level of calculation. Hydrogen-bonds are shown as dotted lines.

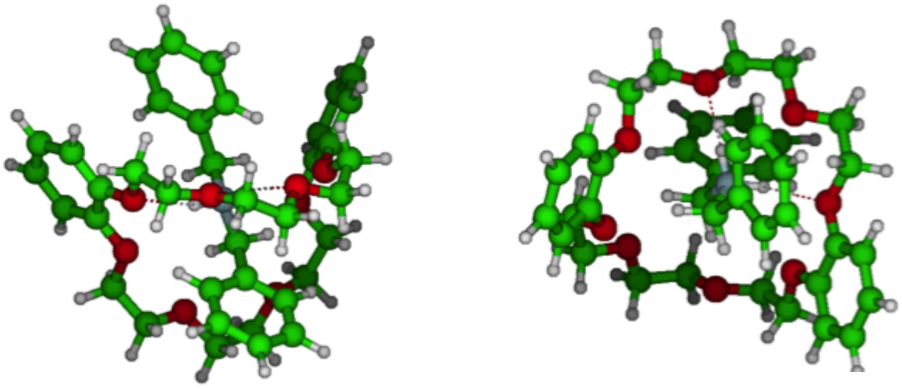

Side View **Top View**

Fig. 9. Most stable structure of dBAM•H^+•DB24C8 pseudo-rotaxane obtained at the M05-2X/6-31+G* level of calculation. Hydrogen bonds between NH and oxygen atom of CE are shown as dotted lines.

The vertical excitation energies and oscillator strengths for the most stable structures of dBAM•H^+, neutral DB24C8, DB24C8•H^+ and dBAM•H^+•DB24C8 obtained at the M05-2X/ 6-31G* level are compared in Table 2. When we compare the S_1-S_0 electronic transition energies of DB24C8 and DB24C8•H^+, and dBAM•H^+, we see that of DB24C8•H^+ is located between those of DB24C8 and dBAM•H^+, which is in good agreement with the observed relationship of the UVPD spectra of Fig. 7. In addition, the S_1-S_0 and S_2-S_0 oscillator strengths of DB24C8•H^+ are ~5 times larger than the dBAM•H^+ oscillator strength, which also agrees with the observed larger photo-fragmentation yield of dBAM•H^+•DB24C8 as compared to that of dBAM•H^+•24C8.

Table 2. Vertical excitation energies (eV) and oscillator strengths (parentheses) of dBAM•H^+, DB24C8, DB24C8•H^+ and dBAM•H^+•dB24C8 rotaxane calculated at the M05-2X/6-31G* level.

	dBAM•H^+ (Open)	DB24C8	DB24C8•H^+	dBAM•H^+• DB24C8
S_1	5.58 (0.0)	5.35 (6.4E-2)	5.42 (4.2E-2)	5.33 (4.7E-2)
S_2	5.59 (9.8E-3)	5.39 (5.0E-2)	5.55 (1.3E-2)	5.40 (4.9E-2)

Conclusion

In summary, we investigated the geometrical and electronic structures of the complex ions of protonated aniline (aniline•H^+) and dibenzylamine (dBAM•H^+) with crown ethers (CEs) of different cavity size, 15C5, 18C6, 24C8, and DB24C8. The aniline•H^+ complexes with 15C5 and 18C6, have a structure in which the proton is located on the aniline part. After UV excitation, the complexes relax to the ground electronic state and the proton is transferred from the aniline part to the CE moiety producing the protonated CE fragments. The cage effect here completely removes the dissociation channels of the aniline•H^+ moiety, which is different from what was observed for the tryptamine•H^+•18C6 complex. In addition, the UV spectrum of aniline•H^+•CE is very sensitive to the symmetry of CE; aniline•H^+•18C6 shows sharp electronic spectrum similar to aniline•H^+, while that of aniline•H^+•15C5 shows very broad structure with poor Franck-Condon factors.

For the dBAM•H^+ complexes with CE, the proton is always located on dBAM. However, CE has a role of proton acceptor, leading to the blue-shift of electronic transition. Actually, in the case of DB24C8, the transition of DB24C8 moiety of dBAM•H^+•DB24C8 is ~ 800 cm-1 blue-shifted compared to neutral DB24C8.

A large difference in the fragmentation yield between dBAM•H^+•18C6 and dBAM•H^+•24C8 was found due to a large barrier for releasing dBAM•H^+ from the axis

of rotaxane. Whereas in dBAM•H^+•24C8 the excitation is on the $dBAMH^+$ moiety, in dBAM•H^+•DB24C8 the initial excitation is on the $DB24C8H^+$ part and the fragmentation yield is larger in this latter case due to a larger oscillator strength. For further details on the structure of the complexes including the position of the proton, the IR spectrum in the NH and OH region should be measured, which will be the future work.

Acknowledgments

This study was supported in part by the France-Japan Collaboration Program (SAKURA), the Japan Society for Promotion of Science and the ANR Research Grant (ESPEM- ANR2010BLANC040501). We acknowledge the use of the computing facility cluster GMPCS of the LUMAT federation (FR LUMAT 2764).

References

1. C. J. Pedersen, *J. Am. Chem. Soc.,* 1967, **89**, 7017-7036.
2. C. J. Pedersen, *Science,* 1988**, 241**, 536-540.
3. A. M. Stuart and J. A. Vidal, *J. Org. Chem.,* 2007, **72**, 3735-3740.
4. N. Jose, S. Sengupta and J. K. Basu, *J. Mol. Catal. A: Chem.,* 2009, **309**, 153-158.
5. J. Malval, I. Gosse, J. Morand and R. Lapouyade, *J. Am. Chem. Soc.,* 2002, **124**, 904-905.
6. R. M. Uda, T. Matsui, M. Oue and K. Kimura, *J. Inclusion Phenom. Macrocyclic Chem.* 2005, **51**, 111-114.
7. I. F. Uchegbu and S. P. Vyas, *Int. J. Pharm.* 1998, **172**, 33-70.
8. L. Tavano, R. Muzzalupo, S. Trombino, I. Nicotera, C. O. Rossi and C. L. Mesa, *Colloids Surf. B*, 2008, **61**, 30-38.
9. R. M. Izatt, J. H. Rytting, D. P. Nelson, B. L. Hayamore and J. J. Christensen, *Science*, 1969, **164**, 443-444.
10. R. M. Izatt, D. P. Nelson, J. H. Rytting, J. J. Christensen and *J. Am. Chem. Soc.* 1971, **93**, 1619-1623.
11. C. J. Pedersen and H. K. Frensdorff, *Angew. Chem. Int. Ed.* 1972, **11**, 16-25.
12. R. M. Izatt, R. E. Terry, B. L. Haymore, L. D. Hansen, N. K. Dalley, A. G. Avondet, and J. J. Christensen, *J. Am. Chem. Soc.* 1976, **98**, 7620-7626.
13. R. M. Izatt, R. E. Terry, D. P. Nelson, Y. Chan, D. J. Eatough, J. S. Bradshaw, L. D. Hansen and J. J. Christensen, *J. Am. Chem. Soc.* 1976, **98**, 7626-30.
14. J. D. Lamb, R. M. Izatt, C. S. Swain and J. J. Christensen, *J. Am. Chem. Soc.* 1980, **102**, 475-479.
15. S. Maleknia and J. Brodbelt, *J. Am. Chem. Soc.* 1992, **114** , 4295-4298.
16. M. B. More, D. Ray and P. B. Armentrout, *J. Am. Chem. Soc.* 1999**, 121**, 417-423.
17. J. D. Anderson, E. S. Paulsen and D. V. Dearden, *Int. J. Mass Spectrom.* 2003, **227**, 63-76.
18. R. Kusaka, Y. Inokuchi and T. Ebata, *Phys. Chem. Chem. Phys.* 2007, **9**, 4452-4459.
19. R. Kusaka, Y. Inokuchi asnd T. Ebata, *Phys. Chem. Chem. Phys.* 2008, **10**, 6238-6244.
20. R. Kusaka, Y. Inokuchi and T. Ebata, *Phys. Chem. Chem. Phys.* 2009, **11**, 9132-9140.
21. S. Kokubu, R. Kusaka, Y. Inokuchi, T. Haino and T. Ebata, *Phys. Chem. Chem. Phys.* 2010, **12** , 3559-3565.
22. R. Kusaka, Y. Inokuchi, S. S. Xantheas and T. Ebata, *Sensors,* 2010**, 10,** 3519-3548.
23. R. Kusaka, S. Kokubu, Y. Inokuchi, T. Haino and T. Ebata, *Phys. Chem. Chem. Phys.*, 2011, **13,** 6827-6836

24. R. Kusaka, Y. Inokuchi, T. Haino and T. Ebata, *J. Phys. Chem. Letters*, 2012, **3**, 1414–1420
25. Y. Inokuchi, O. V. Boyarkin, R. Kusaka, T. Haino, T. Ebata and T. R. Rizzo, *J. Am. Chem. Soc.* 2011, **133** , 12256-12263.
26. Y. Inokuchi, O. V. Boyarkin, R. Kusaka, T. Haino, T. Ebata and T. R. Rizzo, *J. Phys. Chem. A* 2012, **116**, 4057-4068.
27. Y. Inokuchi, T. Ebata, T. R. Rizzo and O. V. Boyarkin, *J. Am. Chem. Soc.* 2014, **136** , 1815-1824.
28. G. Féraud, M. Broquier, C. Dedonder-Lardeux,. G. Grégoire, S. Soorkia, C. Jouvet, *Phys. Chem. Chem. Phys.* 2014, **16**, 5250-5259
29. J. -P. Desvergne and H. Bouas-Laurent, *J. Chem. Soc., Chem. Commun.*, 1978, 403 - 404,
30. I. Yamashita, M. Fujii, T. Kaneda, S. Misumi and T. Otsubo, *Tetrahedron Letters,* 1980, **21**, 541-544
31. H. Bouas-Laurent, A. Castellan and J.-P. Desvergne, *Pure & Appl. Chem*. 1980, **52**, 2633 - 2648.
32. S. Shinkai, T. Nakaji, Y. Nishida, T. Ogawa and O. Manabe, *J. Am. Chem. Soc.*, 1980, **102**, 5860 - 5865.
33. V. Serreli, C.-F. Lee, E. R. Kay and D. A. Leigh, *Nature*, 2007, **445**, 523-527.
34. P. L. Anelli, N. Spencer, J. F. Stoddart, *J. Am. Chem. Soc.,*1991, **113**, 5131 - 5133.
35. R. A Bissell, E. Córdova, A. E. Kaifer, J. F. Stoddart , *Nature*, 1994, **369**, 133 - 137.
36. C. A. Schalley, K. Beizai, and F. Vögtle, *Chem. Res.,* 2001, **34**, 465-476.
37. I. Alata, J. Bert, M. Broquier, C. Dedonder, G. Feraud, G. Gregoire, S. Soorkia, E. Marceca and C. Jouvet, *J. Phys. Chem. A* 2013, **117**, 4420-4427
38. G. Féraud, C. Dedonder, C.Jouvet, Y. Inokuchi, T. Haino, R. Sekiya, T.Ebata, *J. Phys. Chem. Lett.,* 2014, **5**, 1236-1240
39. X. B. Wang and L. S. Wang, *Rev. Sci. Instrum.* 2008, **79**, 073108
40. C. M. Choi, D. H. Choi, N. J. Kim and J. Heo, *Int. J. Mass Spectrom.* 2012, **314**, 18–21
41. J. U. Andersen, P. Hvelplund, S. B. Nielsen, S. Tomita, H. Wahlgreen, S. P. Møller, U. V. Pedersen, J. S. Forster, T. J. D. Jørgensen, *Rev. Sci. Instrum.* 2002, **73**, 1284–1287
42. M. J. S. Dewar, E. G. Zoebisch, E. F. Healy, J. J. P. Stewart, *J. Am. Chem. Soc*.,

1985, **107**, 3902–3909

43. F. Mohamadi, N. G. J. Richard, W. C. Guida, R. Liskamp, M. Lipton, C. Caufield, G. Chang, T. Hendrickson, W. C. Still, *J. Comput. Chem.* 1990, **11**, 440–467

44. T. A. Halgren, *J. Comput. Chem.*, 1999, **20**, 720-729.

45. E. Polak, G. Ribiere, *Rev. Franç Informat. Rech. Operationnelle*, 1969, **16**, 241-254.

46. M. J. Frisch, G. W. Trucks, H. B. Schlegel, G. E. Scuseria, M. A. Robb, J. R. Cheeseman, G. Scalmani, V. Barone, B. Mennuchi, G. Petersson *et al*., *Gaussian* 09, *Revision A.1*, Gaussian, Inc., Wallingford, CT, 2009.

47. P. R. Ashton, E. J. T. Chrystal, P. T. Glink, S. Menzer, C. Schiavo, N. Spencer, J. F. Stoddart, P. A. Tasker, A. J. P. White and D. J. Williams, *Chem. Eur. J.* 1996, **2**, 709-728.

48. N. Mikami, A. Hiraya, I. Fujiwara, and M. Ito, *Chem. Phys. Lett.*, 1980, **74,** 531–535

49. S. Ishikawa, T. Ebata, H. Ishikawa, T. Inoue, and N. Mikami, *J. Phys. Chem.* 1996, **100***,* 10531-10535.

50. The notation for the vibrational modes is adapted from G. Varsanyi, "*Assignments for Vibrational Spectra of Seven Hundreds Benzene Derivatives*" Adam Hilger, London; 1974.

51. NIST *Chemistry Webbook*, NIST Standard Reference Database Number 69, (http://webbbok.nist.gov./chemistry/).

52. F. M. Pasker, N. Solca, and O. Dopfer, *J. Phys. Chem. A* 2006, **110**, 12793-12804.

53. H. Kang, C. Jouvet, C. Dedonder-Lardeux, S. Martrenchard, C. Charriere, G. Gregoire, C. Desfrancois, J.-P. P. Schermann, M. Barat, J. A. Fayeton, G. Grégoire, and C. Desfrançois, *J. Chem. Phys.*, 2005, **122**, 084307.

54. U. Kadhane, M. Perot, B. Lucas, M. Barat, J. A. Fayeton, C. Jouvet, A. Ehlerding,M.-B. S. B. S. Kirketerp, B. Nielsen S, J. a. A. Wyer, H. Zettergren, and M. Pérot, *Chem. Phys. Lett.*, 2009, **480**, 57–61.

Graphic abstract:

Crown ethers show dramatic effect on the electronic spectra and fragmentation pattern of guest species.